Electron resonant tunneling through a circle-ring multicomponent quantum system

Kouta Sugiyama, Takuma Okunishi, Masakazu Muraguchi,* and Kyozaburo Takeda†
Department of Electrical Engineering and Bioscience, Graduate School of Advanced Science and Engineering, Waseda University, Tokyo 169-8555, Japan

(Received 28 July 2009; revised manuscript received 22 December 2009; published 9 March 2010)

We theoretically study resonant tunneling for an electron injected into a multicomponent quantum (QCR) system composed of a quantum circle (QC) and quantum ring (QR). We first solve the time-independent Schrödinger equation numerically to determine the eigenstates of an electron confined in the QCR with an externally applied electrostatic (gate) potential. Several QC and QR local states hybridize mutually to produce the QCR eigenstates, resulting in crossing and/or avoided crossing of the eigenstates. Interestingly, local orbital hybridization is generated commensurately or incommensurately due to the coaxial geometry in the QCR system. The commensurate state produces a rational bonding-antibonding interaction whereas the incommensurate state causes a discrepancy in the position of the nodal planes of the QC and QR local orbitals. We then solve the time-dependent Schrödinger equation for the electron resonant tunneling through this QCR system computationally and study the dynamical properties based on projection analysis. When the electron is injected asymmetrically into the QCR system, quasidegeneracy in the eigenstates induces interstate interference and causes a characteristic "coming-and-going" variation in the electron density ρ. When the electron is injected into the avoided-crossing states produced by the incommensurate local-orbital mixing, the interstate interference induces a "rotational" motion in ρ in spite of the fact that the electrostatic gate potential is uniformly applied to the system.

DOI: 10.1103/PhysRevB.81.115309 PACS number(s): 73.21.La, 73.22.Dj, 73.23.−b, 73.40.Gk

I. INTRODUCTION

Electrons exhibit two contradictory nature, wave and particle nature. The wave nature arises and strengthens when the electron is confined in a nanometer size space. Enhancement of this wave nature causes interesting phenomena that are unexpected from the classical or particle view. These quantum phenomena can materialize as quantum structures[1] and recent progress in nanotechnology has enabled us to fabricate such systems. An example is the quantum ring (QR), for which Aharonov and Bohm (AB) (Ref. 2) have proposed the possibility of direct observation of the vector potential using the phase interference of the wave functions. Tonomura *et al.*[3] first accomplished this in a pioneering experiment where they confirmed the relative phase shift expected by the AB effect. Advances in the fabrication of self-assembled semiconductor rings[4] have accelerated the intensive and extensive research in this area. As a result, further novel quantum phenomena have been found in conductance and persistent currents.[5,6]

The key to understanding these quantum phenomena is the interference interaction caused by the strengthened wave nature of an electron. The AB effect is generated by the interference of the wave functions, by which a phase difference is produced along the electron propagation paths (phase interference). The interesting quantum phenomena found in conductance and persistent currents[5,6] are also caused by similar quantum interference. In contrast, we have reported another type of interference for an electron confined in a quantum structure.[7] When an electron propagates through a quantum system, resonant tunneling (RT) is generated. An interesting feature is expected when an electron tunnels via several resonant states simultaneously because the multistate tunneling generates interstate interference caused by the different eigenfrequencies. The QR is a typical system that produces this simultaneous RT because the QR has quasidegenerate states. In previous work,[7] we demonstrated that the interstate interference in a QR induces dynamical fluctuation in the electron density because the QR hybridizes the eigenstates having different quantum angular numbers. Particularly, under a static magnetic field, we found that the interstate interference changes the rotational direction of the electron density by varying the strength of the applied static magnetic field only, without changing its applied direction. This feature is in contrast to ordinal cyclotron motion (single eigenstate) where the magnetic field should be applied in the opposite direction to invert the rotation. Thus, the interstate interference is different from the phase interference observed in the AB effect and its derivatives where the interference occurs through the phase difference.

In this paper, we study the novel phenomena caused by the interstate interference and discuss their controllability by tuning the quasidegeneracy of the eigenstates. We study this subject by investigating the resonant tunneling of an electron through a QC and QR multicomponent (QCR) system under the application of an electrostatic (gate) potential. This multicomponent quantum system provides an opportunity to study the hybridization between the two quantum structures systematically because the QCR has a concentricity and the "angular moment" remain as a good quantum number in both these components. This QCR is also the suitable system to induce the rotational motion in the electron density because the irrational orbital mixing feasibly causes the discrepancy in the local-node lines of the quantum components. Considering that the orbital mixing is generated between those having the same irreducible representation and is strengthened when those local orbitals (LOs) have similar eigenenergies, the application of the gate potential has a function to control the above orbital mixings artificially.

Analog quantum systems have been produced using molecular-beam epitaxy for InAs on GaAs.[8,9] More recently, Mano *et al.*[10] have succeeded in the self-assembled formation of concentric quantum double rings (CQDRs) using the droplet epitaxy technique. They found that the growth process condition has a potential to control the individual ring's size. These fabricated CQDRs quite resemble to the present QCR. The resulting high uniformity and excellent rotational symmetry surely produce the characteristically quantized eigenstates whose peculiar nature has been confirmed by the photoluminescence spectra observation. The crucial problems that one should take into account in the consideration are some types of disorders and/or practical dissipations ignored in the ideal system. However, the presently focused interstate interference requests an appearance of quasidegenerated states. Accordingly, any disorders work to produce these quasidegenerated states via the symmetry breaking. Thus, the symmetry breaking in the QCR system is feasible and significant due to its highly rotational symmetry of $D_{\infty h}$. Even the contact of the electron leads breaks the rotational symmetry. Thus, the idea of the multicomponent quantum system considered in the QCR system would be meaningful.

In Sec. II, we numerically determine the eigenstates of the QC and QR components and those of the multicomponent QCR system. We then investigate the characteristics of the electronic structures, focusing on the orbital hybridization between the QC and QR local orbitals. Besides the ordinary bonding and antibonding hybridization (commensurate mixing), we find curious hybridization where the local angular node number (quantum numbers) in the QC does not coincide with that in the QR and vice versa (incommensurate mixing). We also discuss how the applied gate (electrostatic) potential changes the orbital mixings and eigenstates. In Sec. III, we solve the time-dependent (TD) Schrödinger equation computationally and examine the TD features of electron tunneling through the QCR system resonatively. We find that the interstate interference among the avoided-crossing states causes "rotational" fluctuation in the electron density ρ (charge-density wave, CDW) even though the electrostatic (gate) potential is applied to the system uniformly. Projection analysis reveals how the interstate interference is generated, which helps deepen our understanding of the rotational motion of an electron during the RT process.

II. ELECTRONIC STRUCTURE

A. QC and QR components

The eigenfunction $\Psi_l^n(\mathbf{r})$ and the energy eigenvalue E_l^n of an electron confined in the two-dimensional (2D) QC or QD [Fig. 1(a)] can be represented as follows:

$$\Psi_l^n(\mathbf{r}) = \begin{cases} [AJ_l(k_n r) + BY_l(k_n r)]e^{il\theta}/\sqrt{2\pi} & \text{for QR} \\ \dfrac{1}{\sqrt{\pi}|J_{l+1}(z_{n,l})|} J_l(\chi)e^{il\theta} & \text{for QC,} \end{cases} \quad (1)$$

$$E_l^n = \hbar^2 k_{l,n}^2/2m. \quad (2)$$

Here, the symbols J_ℓ and Y_ℓ are the lth order Bessel and Neumann functions, respectively. The expansion coefficients

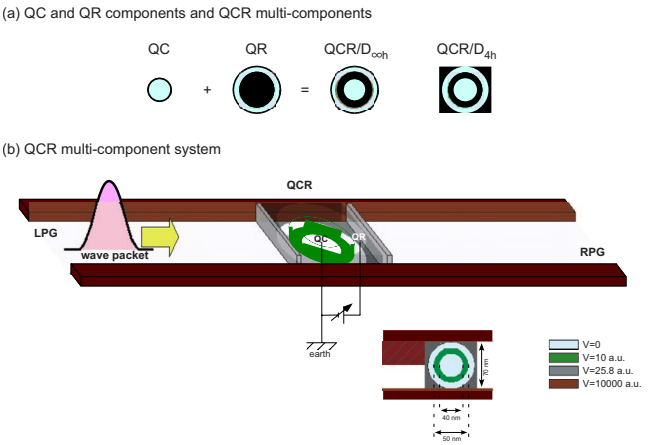

FIG. 1. (Color online) (a) Illustration of the QC and QR components and QCR multicomponent system having a point-group symmetry of $D_{\infty h}$. Also shown is the QCR system surround by four square potential walls (D_{4h}). An electron is confined in the blue (light) area. (b) Illustration of the injection of an electron into the QCR system (D_{2h}) which is connected by wave guides to the left and right. The electrostatic potential is uniformly applied to the component QC and QR via the gate potential and the potential heights are also in the figure. For symmetrical injection, the electron is injected toward the QCR from the left propagation guide (LPG) with the full width of the PG, whereas the LPG is narrowed to half the width by a potential barrier for asymmetrical injection (see also in the inset).

A and B in Eq. (1) should determined by the following boundary condition:

$$\begin{vmatrix} J_l(kr_{in}) & Y_l(kr_{in}) \\ J_l(kr_{out}) & Y_l(kr_{out}) \end{vmatrix} = 0. \quad (3)$$

This secular equation also determines the value of $k(=k_{l,n})$ with an appropriate node suffix n toward the radial direction.

These analytical solutions are, however, valid only when the considered QC and/or QR are isolated in a vacuum to maintain a point-group symmetry of $D_{\infty h}$. The circular hard walls providing these QC and QR are artificially fabricated but the maintaining a geometrical symmetry of $D_{\infty h}$ is not realistic for various reasons; for example, the QC and QR are fabricated from materials that differ from those of the substrate. When the QC and QR are surrounded by four square potential walls to construct the QCR system, this enclosure produces four equivalent corners and lowers the geometrical symmetry of the system from $D_{\infty h}$ to D_{4h}. Connecting the electron propagation guides [PGs in Fig. 1(b)] further lowers the symmetry of the system to D_{2h}. Thus, the doubly degenerate states found in the ideal QC and QR ($D_{\infty h}$) are resolved into $\pm l$ in the present more realistic QCR system [Fig. 1(b)], and the eigenstates of the QC and QR components and also the QCR system can no longer be expressed analytically. Accordingly, numerical calculations are required. Here, we solve the Schrödinger equation computationally to determine the eigenstates $\Phi^{\mathrm{QCR}}(\mathbf{r})$ for an electron confined in the QR or QC components or the QCR system under point-group symmetry of D_{2h}. The numerical calculations are carried out by the finite difference technique, where the wave function is

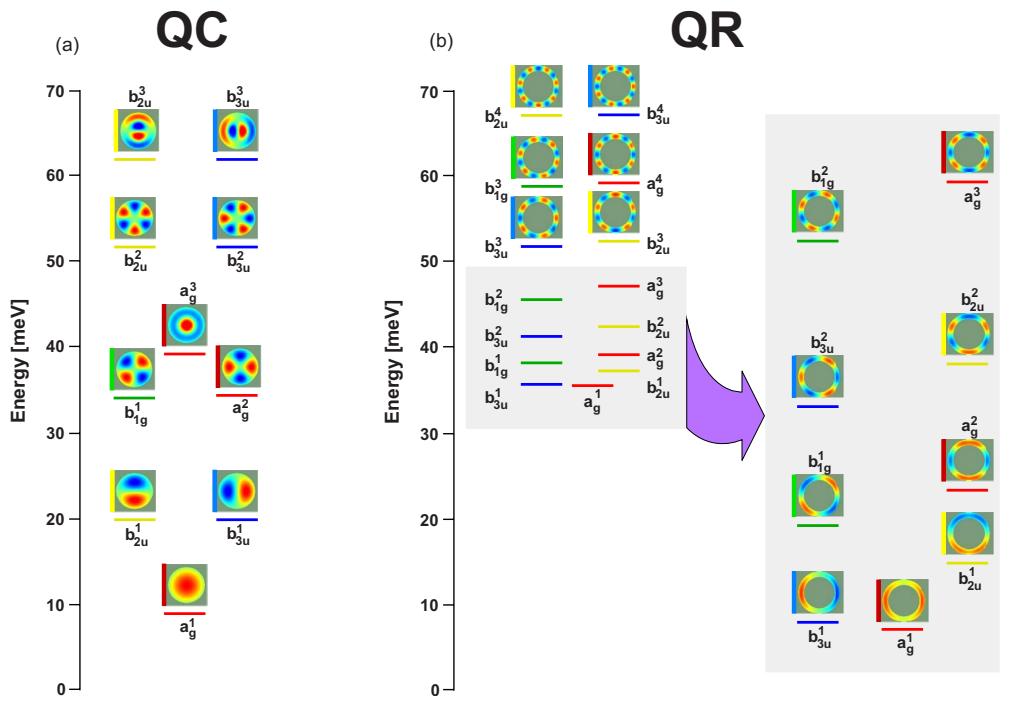

FIG. 2. (Color online) Calculated local eigenstates for an electron confined in (a) an isolated QC and (b) an isolated QR with the corresponding eigenfunctions. We classify these local eigenstates in terms of the irreducible representation by adding the sequential number in the order of the energy, e.g., a_g^1 for the lowest energy state. The eigenstates are also colored in accordance with the orbital symmetry, i.e., red (a_g), blue (b_{3u}), yellow (b_{2u}), and green (b_{1g}), throughout this work.

discretized into real-space grid points. We employ a Cartesian (x and y) grid mesh for the well-ordered execution of the finite difference approach; the square enclosure of the surrounding potential walls promotes the use of this Cartesian grid mesh effectively. In the calculation, we divide the real space into $\Delta x=\Delta y=1/8$ a.u. square grid meshes and set the geometrical parameters for the QR as $r_{in}=25$ and $r_{out}=30$ nm and for the QC we set $r=20$ nm. The heights of the potential barriers are set as shown in Fig. 1. Details of the numerical calculation have been reported in a previous work.[11]

In Fig. 2, we present the calculated eigenstates for the isolated QC and QR components of the present QCR system illustrated in Fig. 1. We note that the lowering of the symmetry (D_{2h}) resolves the degeneracy of the eigenstates into l, resulting in *quasidegenerate* states. The QC gives a ground state a_g^1 having an original quantum number of $(l,n)=(0,1)$. This QC ground state is energetically more stable than the QR ground state by ~25 meV in the present system. We also note that the QC excited state a_g^3, having quantum number $(l,n)=(0,2)$, appears energetically higher than the ground state by ~30 meV, whereas the corresponding QR excited state does not appear up to at least 70 meV (Fig. 2). It is also characteristic that the QR excited states, such as $(l,n)=(\pm1,1),(\pm2,1),(\pm3,1),\ldots$, are densely distributed in energy space than the QC states. These features can be understood by comparing the electron confinement in the radial direction with the direction along the circular angle. In the present QCR geometry, the radial confinement in the QR is at most 10 nm whereas that in the QC is 20 nm, twice as large. Thus, the electron confinement weakened radially in the QC stabilizes its ground and other states having higher radial quantum number "n" energetically compared with those in the QR. In contrast, the QR always has a longer circumference than that of the QC because the QR surrounds the QC coaxially and therefore the QR sets the eigenstates having higher angular quantum number "l" more densely distributed in energy space than those eigenstates of the QC.

B. QCR multicomponent system

We now study the eigenstates of the QCR multicomponent system where the QC and QR are set coaxially and the separating potential is finite [Fig. 1(a)]. Figures 3(a) and 3(b) show the numerically calculated eigenvalues and wave functions, respectively. Similar to those found for the components QC and QR, we find quasidegeneracy in the resulting states owing to the original circular symmetry. We also note that the resulting wave functions of the ground (A_g^1) and lower excited states $(B_{3u}^1$ and $B_{2u}^1)$ are strongly localized within the QC component whereas those of the higher states are well shared both by the components QC and QR [Fig. 3(b)].

The nature of the electron localization/delocalization is well understood by considering the mixing between the QC and QR local orbitals because the potential wall separating the components is now changed into a finite potential of $V_s=10$ a.u. (=116.1 meV) and these local orbitals can interact mutually to create the QCR coherent eigenstates. However, less orbital hybridization is found in the resulting QCR ground state (A_g^1) even though the QC and QR ground states have the same orbital symmetry (a_g). This is because the QC ground state is energetically far from the QR ground state.

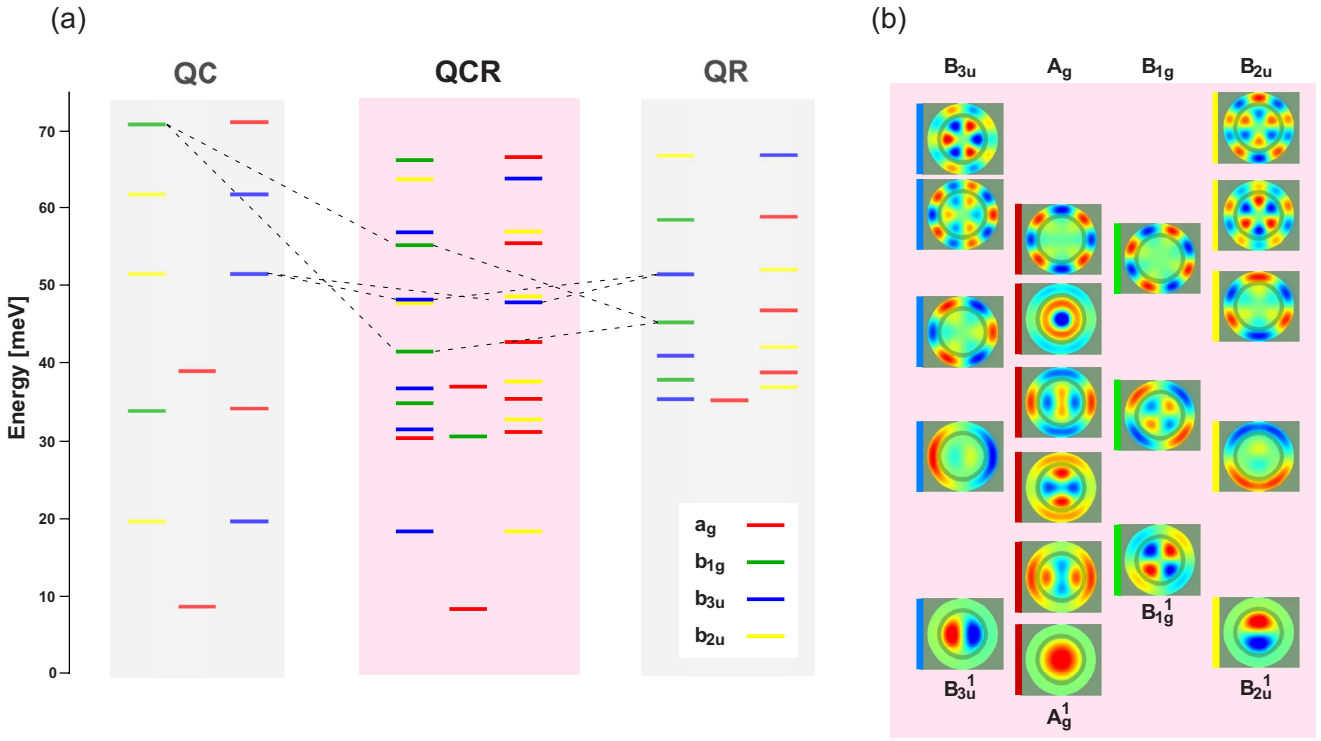

FIG. 3. (Color online) Calculated (a) eigenvalues and (b) eigenstates for an electron confined in the nonbiased QCR system. We classify these local eigenstates in terms of the irreducible representation by adding the sequential number in the order of the energy. We use capital letters in the irreducible representations, such as A_g^1 for the lowest energy state, to distinguish them from the local orbitals of the QC and QR.

Consequently, the resulting QCR ground state localizes at the QC component. Similarly, orbital hybridization hardly occurs in the lower excited states of B_{3u}^1 and B_{2u}^1 in which an electron localizes also in the QC part. In contrast, typical orbital mixing is found in the resulting QCR states B_{1g}^1 and B_{1g}^2. These are caused by the bonding-antibonding interaction between the local orbitals having an orbital symmetry of b_{1g} and a completely identical/opposite phase relation is found between the QC and QR components (*commensurate mixing*). The orbital mixing in the present QCR multicomponent system causes further curious eigenstates where the resulting angular node numbers are different between the components (*incommensurate mixing*). The eigenstates, B_{3u}^4 and B_{3u}^5 and also B_{2u}^4 and B_{2u}^5 are typical examples where the QR part has five angular nodes whereas the QC part has three. We illustrate this incommensurate mixing in Fig. 4 and discuss its characteristics in the next section.

C. Application of electrostatic gate potential

We now consider what happens when the relative energetic positions of the QC and QR are varied. This effect is achieved by applying an electrostatic (gate) potential V external to the present QCR system (biased QCR), as shown in Fig. 1(b). The applied gate potential V does not change the geometrical symmetry of the QCR but varies the energetic position of the QC and QR local orbitals relatively.[12] Consequently, the orbital hybridization is controllable by tuning V. Figure 5 shows the V dependence of the resulting eigenstates of the biased QCR system. The eigenstates at $V=0$ correspond to those given in Fig. 3(a). The resulting eigenstates exhibit V independence as well as V linear dependence in accordance with the applied bias V. Accordingly, the resulting eigenstates intersect mutually and level crossings are produced. Interestingly, these level crossings can be classified into a *simple crossing* and an *avoided crossing* (Appendix A). We can easily understand that the eigenstates are accidentally degenerate at the crossing, whereas the orbital mixing occurs at the avoided crossing where the bonding and

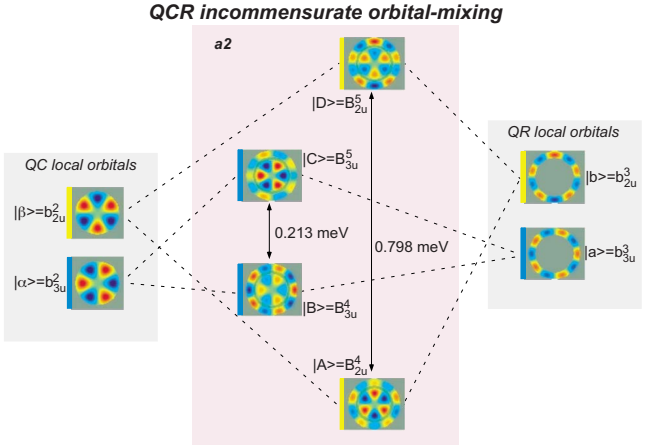

FIG. 4. (Color online) Illustration of incommensurate orbital mixing at point *a*2 (Fig. 5), where the quasidegenerate local orbitals hybridize mutually to cause an avoided crossing. We show the resulting QCR eigenstates with their original local orbitals. The notation in the wave function is described in Sec. III C and Appendix B.

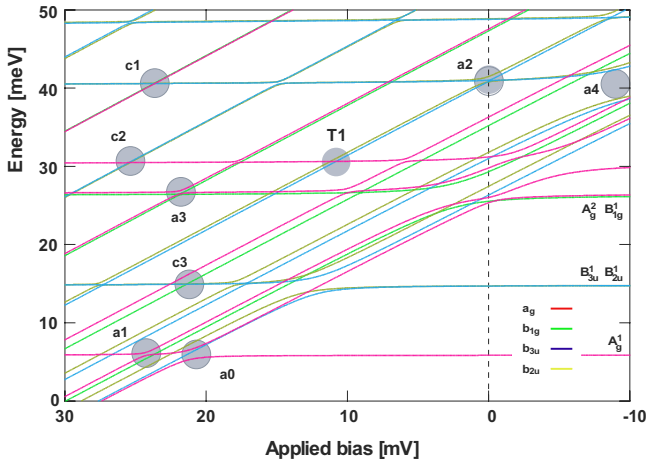

FIG. 5. (Color online) Change in the eigenstates against the applied electrostatic potential (gate potential V) in the biased QCR system. The calculated eigenstates are colored in accordance with the orbital symmetry and several irreducible representations are indicated in the figure. The electrostatic field is externally applied to the QR component while the QC component is connected to the ground directly. Several simple crossings and avoided crossings are indicated by the symbols c and a with the identification number.

antibonding states are produced to delocalize over the QCR system.

We discuss the V dependence, focusing on how and where the eigenstate localizes and/or delocalizes. When the QR is biased negatively to the QC, the lower five states (A_g^1, B_{3u}^1, B_{2u}^1, A_g^2, and B_{1g}^1) cause a V independence, as shown in Fig. 5. As mentioned in Sec. II A, the lower QC eigenstates are more stable and energetically far from the QR eigenstates due to weak electron confinement. Consequently, the QC eigenstates become those QCR eigenstates without the QC-QR orbital hybridization. Thus, these lower five eigenstates localize at the QC component and show V independence because the QC component is connected to the ground directly. In contrast, the completely opposite behavior is found when the QR component is biased positively because the energetic separation is now reduced sufficiently to generate QC-QR orbital mixing. The lowest eigenstate A_{1g}^1, as an example, localized at the QC component now delocalizes over the QCR system at the avoided crossing $a0$ and then localizes at the QR area after passing $a0$. That is, this state changes its V dependence from independence to a linear dependence (Fig. 5).

We study the characteristics of the electronic structures found at several avoided crossings and crossings. We first focus on the avoided crossing found around $V=22.5$ meV ($a0$ in Fig. 5), whose QCR orbitals are illustrated in Fig. 6 with the corresponding QC and QR local orbitals. Figure 6 reveals that local-orbital mixing between the QC and QR causes a rational bonding-antibonding interaction (commensurate mixing); the QCR eigenstate of A_g^1 corresponds to the bonding state and that of A_g^2 corresponds to the anitibonding state. We find another type of avoided crossing at $a1$ when a positive bias is applied to the QR (Fig. 5). Figure 6 demonstrates that a corresponding orbital mixing is caused between the local orbitals of a_g^1 (QC) and a_g^2 (QR), whose original quantum numbers are $(l,n)=(0,1)$ and $(2,1)$, respectively. That is, the QC local orbital has no nodal planes whereas the QR orbital has four planes. Accordingly, the bonding and antibonding nature are now indistinguishable and the energy separation is reduced in the resulting QCR states due to the incommensurate mixing. We also note that the lower QCR state (A_g^2) localizes at the QR whereas the higher QCR state (A_g^3) localizes at the QC (Fig. 6). This is why the former shows a V linear dependence whereas the latter shows V independence when a further positive external potential is applied (Fig. 5).

These commensurate and incommensurate mixings arise irrespective of the nondegeneracy/quasidegeneracy in the local orbitals, as shown in Fig. 6. We now discuss the electronic structure at the avoided-crossing point $a4$, where the QR is now biased negatively relative to the QC. The local orbitals of both the QC and QR are quasidegenerate into b_{2u}^2 and b_{3u}^2 but are classified originally into the degenerate states having $(l,n)=(\pm 3,1)$. The commensurate mixing is then generated, causing the rational bonding-antibonding interaction, as shown in Fig. 6. In contrast, we can also observe incommensurate mixing at the avoided crossing $a3$ where the QC local orbitals are quasidegenerate into a_g^2 and b_{1g}^1 having four angular nodal planes, whereas the QR local orbitals (a_g^4 and a_g^3) have 12 angular nodal planes. Eventually, the rational bonding-antibonding interaction disappears in the resulting quasidegenerate QCR states (Fig. 6).

Now we discuss the electronic structures found at the crossings $c1$, $c2$, and $c3$ as shown in Fig. 7. The QCR eigenstates at the crossings have different orbital symmetries but the same eigenvalues. Thus, there is an accidental degeneracy. We should note the following: $c3$ is composed of three QCR eigenstates B_{3u}^3, B_{2u}^3, and B_{1g}^2, though the former two states are degenerate originally because $(l,n)=(\pm 1,1)$ under the point-group symmetry $D_{\infty h}$. Thus, the eigenstates B_{3u}^3 and B_{2u}^3 localize at the QC whereas the B_{1g}^2 state localizes at the QR (Fig. 7). Consequently, the former two states exhibit V independence, whereas the latter exhibits linear V dependence (Fig. 5). An analogous accidental degeneracy is found at the other crossings $c1$ and $c2$. The crossing point $c1$ is composed of four eigenstates A_g^8, B_{1g}^5, B_{3u}^6, and B_{2u}^6. The former and latter two states are strictly quasidegenerate, though they localize at each component of the QR and the QC, respectively. Eventually, typical V linear dependence should appear in the former two states whereas less V dependence is found in the latter, as shown in Fig. 5. Similarly, the linear V dependence of the quasidegenerate states B_{3u}^5 and B_{2u}^6 equalizes their eigenvalues to that of the A_g^7 state and causes accidental degeneracy at $c2$ (Appendix A).

III. RESONANT TUNNELING

A. Transimittance

Here, we study the dynamical properties of an electron injected toward the QCR as shown in Fig. 1(b) (hereafter, symmetrical injection). We inject an electron from the left propagating guide into the QCR as a wave packet having the following Gaussian form:

$$\psi(x,y;t=0) = D\exp\left[-i\frac{p_x}{\hbar}(x-x_0)\right] \times \exp\left[-\frac{(x-x_0)^2}{2\sigma^2}\right]\cos\left[\frac{\pi(y-y_0)}{L_y}\right]. \quad (4)$$

Here, we modify the plane wave as $\exp[-i\frac{p_x}{\hbar}(x-x_0)]$ in order to represent the electron propagation in the x direction with momentum p_x while a cosine-type standing wave is assumed to expand in the y (vertical to the propagating) direction. We set the electron wave packet at the initial point (x_0, y_0) with a real-space distribution σ of a Gaussian form (σ=160 nm). We assign a normalized constant to D for the wave packet described by Eq. (4). We tune the initial kinetic energy to agree with the target resonant state(s) E_{RS} based on the following equation:

$$E_{RS} = \frac{\hbar^2}{2m^*}\left(k_0^2 + \frac{1}{2\sigma^2}\right).$$

We obtain the total transmittance T of an electron through the present system by varying its kinetic energy in the injection. We calculated the probability density T (Fig. 8) in the right-side PG area after sufficient time had passed after the electron injection. We can determine the characteristic peaks in the transmittance whose energy values are in agreement with those eigenvalues of the corresponding resonant states (Fig. 3). The resulting transmittance reveals that the injected wave-packet tunnels via the resonant states having an orbital symmetry of a_g or b_{3u} but never tunnels via the resonant states having symmetry b_{2u} and b_{1g} because we initially inject the nodeless wave packet (n_y=0) in the y direction. That is, the tunneling states should have an even symmetry in the y direction for the present symmetrical injection. The strongest peak is caused by threefold quasidegenerate states of A_g^2, A_g^3, and B_{3u}^2. The second large peak found around 33 meV has a shoulder in the higher energy region, which is caused by the resonant states of A_g^4 and B_{3u}^3, as shown in Fig. 8. The present dispersion (σ=317.4 nm) of the injected wave packet enforces these individual peaks indistinguishably. It is also a characteristic that the resonant states localizing at the outer QR component tend to cause a higher transmittance compared with those localizing at the inner QC component.

B. Symmetrical injection

As discussed in Sec. II, the resonant states in the present QCR system are distributed highly densely in energy so that it is difficult to distinguish the target resonant state(s) from others for the electron tunneling. However, the application of the gate potential allows them to be distinguished. Thus, we can inject an electron into the desired resonant states. Here,

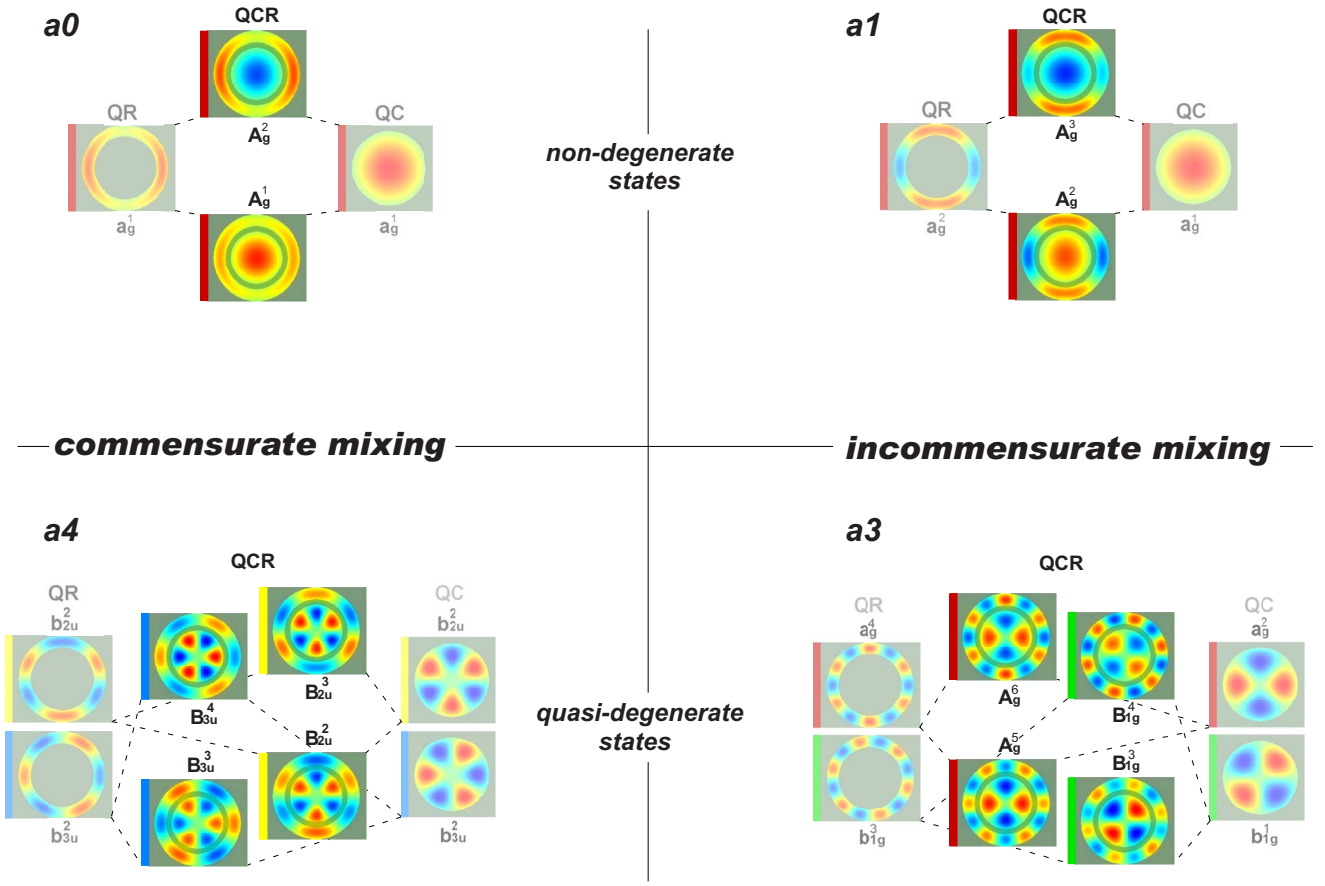

FIG. 6. (Color online) Illustration of the eigenfunctions at the avoided crossings $a0$, $a1$, $a3$, and $a4$. The former two are caused by the nondegenerate local orbitals and the latter two are caused by the quasidegenerate local orbitals. They can also be classified into commensurate ($a0$ and $a4$) and incommensurate mixing ($a1$ and $a3$).

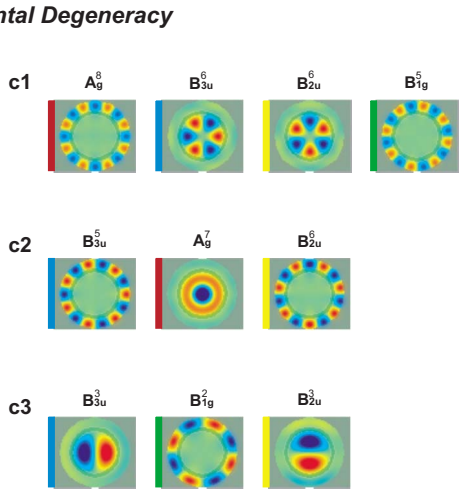

FIG. 7. (Color online) Illustration of the eigenfunctions at the crossings $c1$, $c2$, and $c3$. The accidental degeneracy maintains the electron localization of the local orbitals without orbital hybridization.

we inject an electron symmetrically into the resonant states $T1$ as shown in Fig. 5, where three eigenstates B^4_{3u}, B^4_{2u}, and A^6_g are accidentally degenerate.[13]

Figure 9 shows the change in the total charge (electron) density $\rho^{\mathrm{T}}(=\langle\Phi^{\mathrm{QCR}}(\mathbf{r},t)|\Phi^{\mathrm{QCR}}(\mathbf{r},t)\rangle_{\mathrm{QCR}})$ against the propagation time t. We also show the partial charge densities $\rho^{\mathrm{QC}}(=\langle\Phi^{\mathrm{QCR}}(\mathbf{r},t)|\Phi^{\mathrm{QCR}}(\mathbf{r},t)\rangle_{\mathrm{QC}})$ and $\rho^{\mathrm{QR}}(=\langle\Phi^{\mathrm{QCR}}(\mathbf{r},t)|\Phi^{\mathrm{QCR}}(\mathbf{r},t)\rangle_{\mathrm{QR}})$ in the figure. The value of ρ^T increases steeply and then reaches a maximum when $t\sim 2.5$ ps. Successively, it decreases with a typical exponential reduction with a lifetime of $\tau\sim 7.6$ ps. This feature indicates that the injected electron tunnels through the QCR system resonatively. The decomposition of ρ^{T} into ρ^{QC} and ρ^{QR} reveals that the injected electron tunnels mainly through the QR whereas the electron remaining in the QC area causes a long tail in the total TD profile. The small value of ρ^{QC} indicates that the contribution from electrons inflowing from QR to QC via tunneling is not significant. Conversely, it means that there is little outflow from QC to QR, which is why the partial density at the QC (ρ^{QC}) does not reduce rapidly but has a long lifetime.

To clarify these characteristic features, we employ projection analysis[7,11] in which the calculated TD wave function is projected into the QCR resonant orbitals $[\phi_i^{\mathrm{QCR}}(\mathbf{r})]$ or the QR and QC local orbitals $[\phi_i^{\mathrm{QC}}(\mathbf{r})$ and $\phi_i^{\mathrm{QR}}(\mathbf{r})]$. In Fig. 9(b), we give the expansion coefficient $[C_i^{\mathrm{QCR}}(t)=\langle\Phi^{\mathrm{QCR}}(\mathbf{r},t)|\phi_i^{\mathrm{QCR}}(\mathbf{r})\rangle_{\mathrm{QCR}}]$ obtained by the inner product between the TD wave function $\Phi^{\mathrm{QCR}}(\mathbf{r},t)$ and the QCR resonant states $\phi_m^{\mathrm{QCR}}(\mathbf{r})$ against time t. The injected electron tunnels the QCR system mainly via the two resonant states B^4_{3u} and A^6_g, although we injected the electron at the crossing point $T1$ having a threefold accidental degeneracy among B^4_{3u}, A^6_g, and B^4_{2u}. This selective tunneling is caused by the conservation of the orbital parity due to the geometrical symmetry.[14] We also note that the resulting TD feature in the projection coefficient $|C_i^{\mathrm{QCR}}(t)|^2$ ($i=B^4_{3u}$ and A^6_g) is coincident with the partial density of ρ^{QR} and ρ^{QC}, respectively. Both $|C_i^{\mathrm{QCR}}(t)|^2$ reach their maxima at $t\sim 5$ ps but have significant differences in their values ($\sim 10:1$), similar as that found for ρ^{QR} and ρ^{QC} [Fig. 9(a)]. This feature is caused by the geometrical localization of the individual resonant states at the crossing point $T1$. These three states are mutually orthogonal and any hybridizations are not generated among them due to the threefold accidental degeneracy.[15] Consequently, the QCR resonant states maintain their original nature of the QC and QR local orbitals which they had before the accidental degeneracy occurs. That is, the tunneling via the resonant state B^4_{3u} approximates to that via the QR local orbital b^3_{3u} and the tunneling via the resonant state A^6_g approximates to that via the QC local orbital a^3_g. The strong localization in these component orbitals reduces the tunneling probability between QR and QC significantly. Accordingly, the electron injected in the QR hardly intrudes into the QC and also barely comes out from the QC. This small overlap $\langle B^4_{3u}|A^6_g\rangle\sim\langle b^3_{3u}|a^3_g\rangle\ll 1$ also explains why ρ^{QC} is very small but has a long lifetime. These features can be well understood by employing the local-orbital projection coefficients $|C_i^{\mathrm{QC}}(t)|^2(=|\langle\Phi^{\mathrm{QCR}}(\mathbf{r};t)|\phi_i^{\mathrm{QC}}(\mathbf{r})\rangle|^2)$ and $|C_i^{\mathrm{QR}}(t)|^2(=|\langle\Phi^{\mathrm{QCR}}(\mathbf{r};t)|\phi_i^{\mathrm{QR}}(\mathbf{r})\rangle|^2)$. Figures 9(c) and 9(d) demonstrate that the local-orbital projection coefficients $|C_i^{\mathrm{QC}}(t)|^2$ and $|C_i^{\mathrm{QR}}(t)|^2$ coincide with the corresponding projection coefficient $|C_i^{\mathrm{QCR}}(t)|^2$ when the electron is injected into the crossing point caused by the accidental degeneracy. That is, the resulting TD features in ρ^{QR} and ρ^{QC} are represented in terms of the QC and QR local orbitals.

We now consider fluctuation in the charge density. We have found[7] that the interstate interference induces the characteristic fluctuation in the charge density when the electron tunnels through two or more (quasi)degenerate resonant states. However, no fluctuations are found in the symmetrical

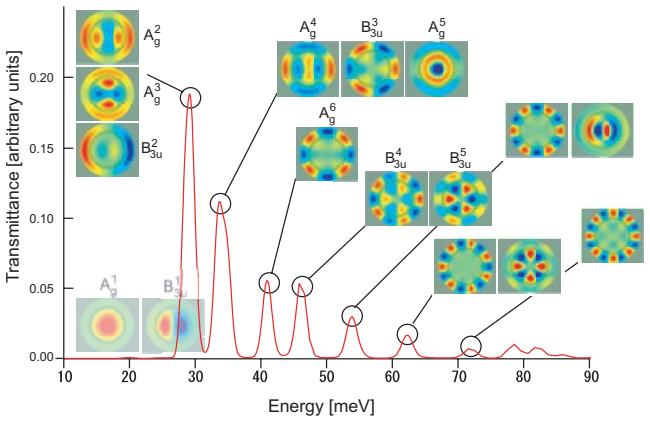

FIG. 8. (Color online) Calculated transmittance of an electron (wave packet) injected into the nonbiased QCR system, varying the initial kinetic energy as indicated by the horizontal axis. The transmittance peaks are assigned to QCR eigenstates directly by indicating their wave functions. It is difficult to find the transmittance peak corresponding to the ground (A^1_g) and first excited (B^1_{3u}) states, although these states have orbital symmetries of a_g and b_{3u}, respectively. This is because their energy eigenvalues are so small that the wave packet having the corresponding kinetic energy does not intrude into the QCR effectively. We also note that the peak height reduces monotonically against the energy. This feature is in contrast to those found in the simple double barrier structure where the observed resonant peaks increase monotonically with energy.

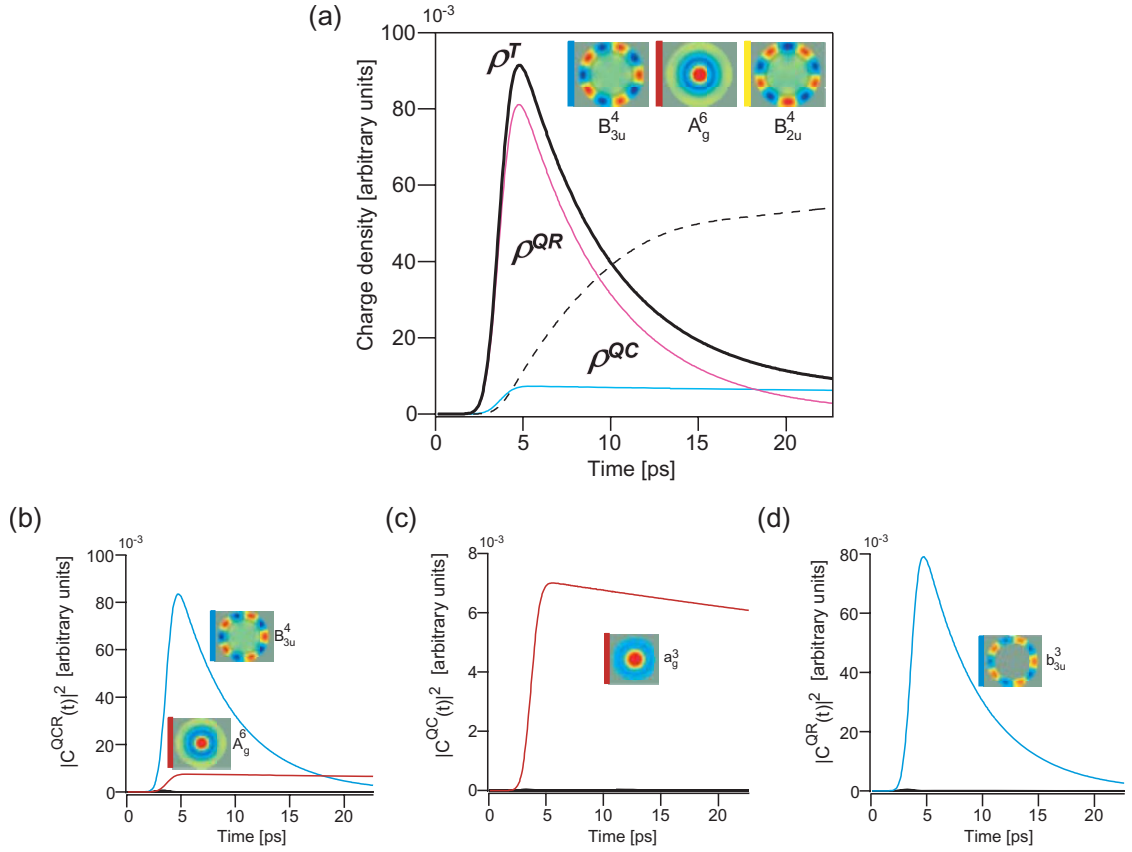

FIG. 9. (Color online) (a) TD features in the total and partial charge (electron) densities when the electron is injected symmetrically into the resonant states $T1$ in Fig. 5. Also shown are the projection coefficients $C_i^{\mathrm{QCR}}(t)$ in (b), $C_i^{\mathrm{QC}}(t)$ in (c), and $C_i^{\mathrm{QR}}(t)$ in (d). The TD feature of the total transmittance is indicated by a broken line in (a).

injection (Fig. 9), although the present electron injected symmetrically into the QCR tunnels via the two resonant states A_g^6 and B_{3u}^4 simultaneously. This is because the fluctuation frequency is given by $\omega_{ij}=\omega_i-\omega_j$, where ω_i is the eigenfrequency of the ith resonant state, though the accidental degeneracy equalizes the eigenfrequencies strictly and gives $\omega_{ij}=0$.

C. Asymmetrical injection

We now inject the electron wave packet asymmetrically upon the QCR using the half-width PG as shown in Fig. 1(b) (asymmetrical injection). For a comparison with the above symmetrical results, we first inject an electron into the target point $T1$. Figure 10(a) shows the TD feature of the total charge density ρ^{T} along with the partial densities ρ^{QR} and ρ^{QC}. The following are conserved even under asymmetrical injection: ρ^{QR} controls the TD feature of ρ^{T} whereas ρ^{QC} is around a tenth of ρ^{QR} but has a long lifetime. We note however that the total and partial charge densities fluctuate against the propagating time with certain frequencies.

We present the projection coefficients $|C_i^{\mathrm{QCR}}(t)|^2$ in Fig. 10(b), showing that the injected electron now tunnels through the QCR via all three resonant states A_g^6, B_{3u}^4, and B_{2u}^4, constructing crossing point $T1$. Figure 10(b) further demonstrates that the electron tunnels most effectively via the resonant state B_{2u}^4, although the tunneling under the symmetrical injection is completely forbidden due to the parity conservation in the orbitals. For asymmetrical injection, we also note that the tunneling via the resonant state B_{3u}^4 is reduced significantly to be comparable to that via the resonant state A_g^6. In Figs. 10(c) and 10(d), we also show the projection coefficients for the QC and QR local orbitals $|C_i^{\mathrm{QC}}(t)|^2$ and $|C_i^{\mathrm{QR}}(t)|^2$, respectively. These figures indicate that the electron tunnels through the QC component via the QC local orbital a_g^3 whereas it tunnels through the QR component via the two QR local orbitals b_{2u}^3 and b_{3u}^3. Similar to symmetrical injection, the TD features of $|C_i^{\mathrm{QC}}(t)|^2$ and $|C_i^{\mathrm{QR}}(t)|^2$ basically agree with those of $|C_i^{\mathrm{QCR}}(t)|^2$ [Fig. 10(b)] having the same orbital symmetry (i). This agreement is due to the strong localization of the QCR resonant states into the individual components and is an important characteristic of the crossing point, as mentioned in Sec. III B. However, in contrast to symmetrical injection, obvious fluctuation is found in the projection coefficients $|C_i^{\mathrm{QCR}}(t)|^2$, $|C_i^{\mathrm{QR}}(t)|^2$, and $|C_i^{\mathrm{QC}}(t)|^2$ and also in the charge densities ρ^{T}, ρ^{QC}, and ρ^{QR}. This is caused by interstate interference[7] because accidental degeneracy at the point $T1$ is generated between the resonant states of A_g^6 and B_{3u}^4 and between A_g^6 and B_{2u}^4, though the two resonant states B_{3u}^4 and B_{2u}^4 form the avoided crossing. Consequently, these two (quasidegenerate) resonant states generate interstate interference having a frequency determined by the energy difference $\omega_{ij}(=\omega_i-\omega_j)$, where $|i\rangle=B_{2\mathrm{u}}^4$ and $|j\rangle=B_{3\mathrm{u}}^4$. Figure 5 confirms that the corresponding energy separation is

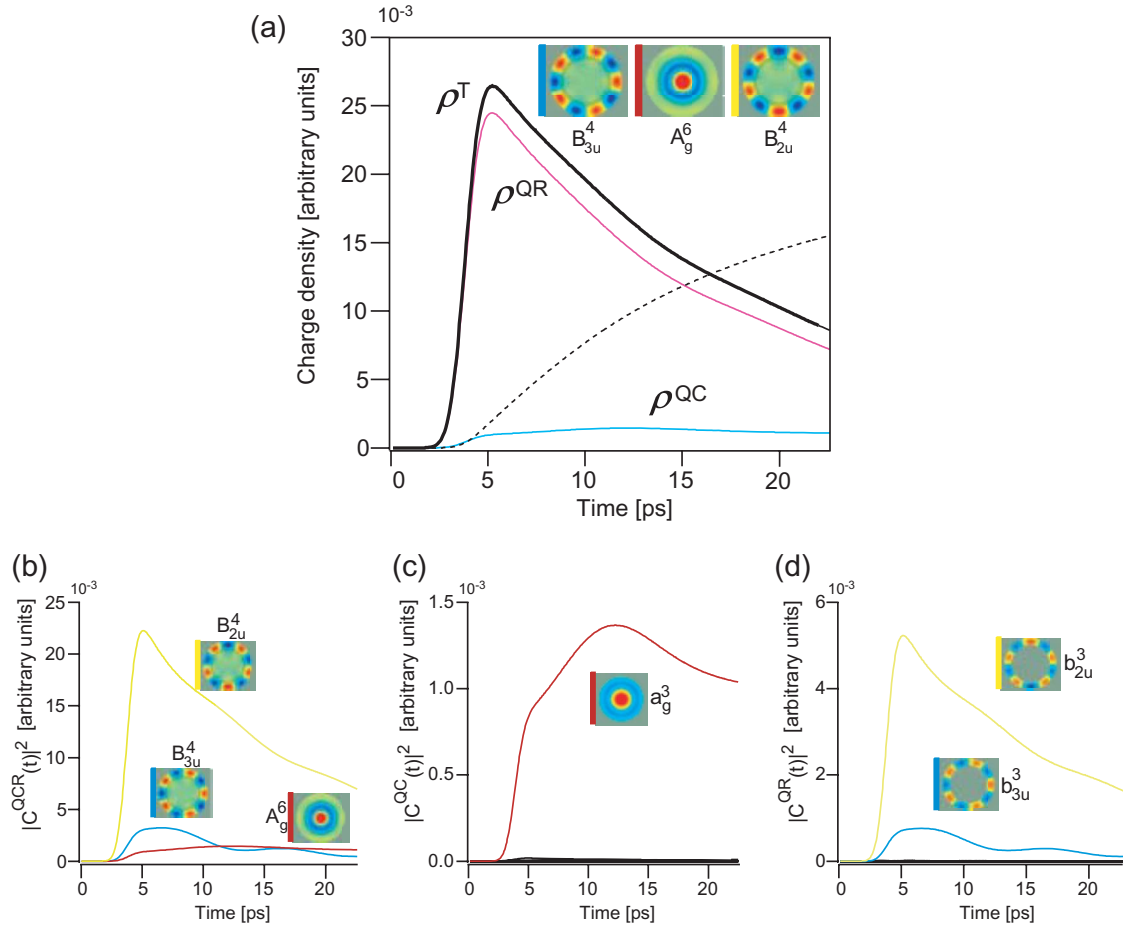

FIG. 10. (Color online) (a) TD features in the total and partial charge (electron) densities when the electron is injected asymmetrically into the resonant states $T1$ in Fig. 5. Also shown are the projection coefficients $C_i^{\mathrm{QCR}}(t)$ in (b), $C_i^{\mathrm{QC}}(t)$ in (c), and $C_i^{\mathrm{QR}}(t)$ in (d). The TD feature of the total transmittance is indicated by a broken line in (a).

small (~0.2 meV) due to the quasidegeneracy. This is why the projection coefficients fluctuate with low frequency; period $T \sim 20$ ps, as observed in Figs. 10(c) and 10(d), would be a reasonable value. We further note that the electron injected asymmetrically also tunnels via other states, slightly though definitely, in addition to the above three eigenstates. The tunneling via these states should induce other frequencies in the fluctuation.

To study the characteristic fluctuations in the charge density, we injected[16] an electron asymmetrically into the avoided-crossing point $a2$ (Fig. 5), where the resonant states B^4_{3u}, B^5_{3u}, B^4_{2u}, and B^5_{2u} are generated by the incommensurate mixing between the QR and QC local orbitals. At the point $a2$, these local orbitals are quasidegenerate into b^3_{3u} and b^3_{2u} (QR) and into b^2_{3u} and b^2_{2u} (QC), as shown in Fig. 4. Figure 11(a) indicates that the total charge density ρ^T increases steeply within a very short time (less than 2 ps) and then reduces gradually exhibiting characteristic plateaus periodically, whereas the partial charge densities ρ^{QC} and ρ^{QR} cause typical sinusoidal fluctuations against time with a single frequency seemingly but with the opposite phase of π. Based on this feature we conclude that the electron injected in the QCR causes a *coming-and-going* motion between the components QC and QR. The calculated snapshots demonstrate this phenomenon as shown Fig. 12(a).[17] When the time is $t \sim 5$ ps (A), an electron localizes at the QC area, whereas it localizes at the QR when $t \sim 7.5$ ps (B). The electron then delocalizes over the QCR system when $t \sim 9$ ps (C). This space-time fluctuation in ρ^{T}, however, is peculiar because the QCR resonant states at the avoided crossing do not localize in either of the components but delocalize over the QCR system.

The projection analysis demonstrates how the interstate interference causes this coming-and-going motion in ρ^{T}. According to Appendix B, the projection analysis employing the QC and QR local orbitals approximates the partial charge densities ρ^{QC} and ρ^{QR} as follows:

$$\rho^{\mathrm{QR}} = \langle \Phi^{\mathrm{QCR}}(\mathbf{r};t) | \Phi_i^{\mathrm{QCR}}(\mathbf{r};t) \rangle_{\mathrm{QR}} = \sum |K_i|^2 + 2|K_B^* K_C|^2 \cos\, \omega_{\mathrm{CB}} t + 2|K_A^* K_D|^2 \cos\, \omega_{\mathrm{DA}} t, \tag{5}$$

$$\rho^{\mathrm{QC}} = \langle \Phi^{\mathrm{QCR}}(\mathbf{r};t) | \Phi_i^{\mathrm{QCR}}(\mathbf{r};t) \rangle_{\mathrm{QC}} = \sum |\kappa_i|^2 + 2|\kappa_B^* \kappa_C|^2 \cos(\omega_{\mathrm{CB}} t + \pi) + 2|\kappa_A^* \kappa_D|^2 \cos(\omega_{\mathrm{DA}} t + \pi). \tag{6}$$

Here, K_i and κ_i are expansion coefficients for the QC and QR local orbitals (Appendix B) and ω_{CB} and ω_{DA} are the fre-

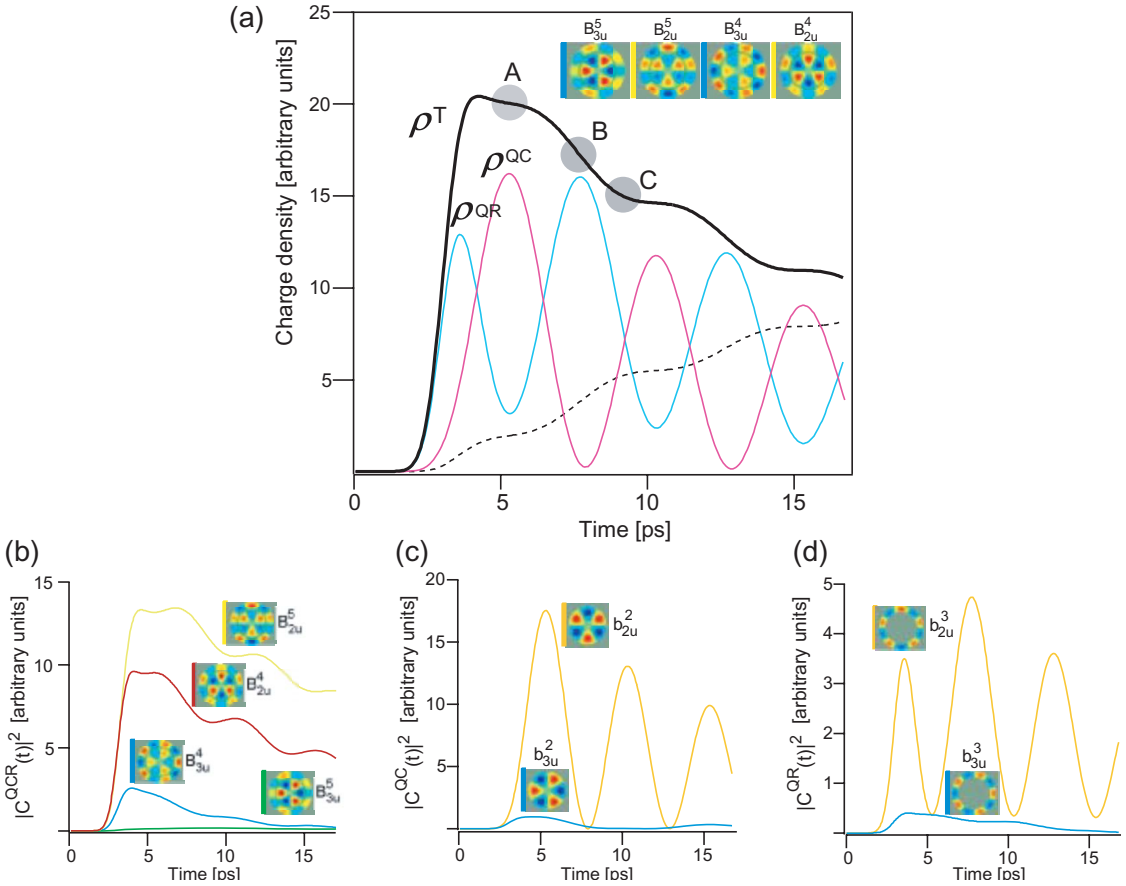

FIG. 11. (Color online) (a) TD features in the total and partial charge (electron) densities when the electron is injected asymmetrically into the resonant states $a2$ in Fig. 5. Also shown are the projection coefficients $|C_i^{QCR}(t)|$ in (b), $|C_i^{QC}(t)|$ in (c), and $|C_i^{QR}(t)|$ in (d). The TD feature of the total transmittance is indicated by a broken line in (a).

quencies determined by the energy difference between the QCR resonant states having the same orbital symmetry as shown in Fig. 4. Equations (5) and (6) reveal that both the partial densities ρ^{QR} and ρ^{QC} oscillate with a frequency derived from ω_{CB} and ω_{DA} but with the opposite phase of π against time. Thus, the coming-and-going nature of $\rho^T(=\rho^{QR}+\rho^{QC})$ is well demonstrated. To be exact, a characteristic beating is induced in ρ^{QR} and ρ^{QC} (and also ρ^T) although their fluctuations found in Fig. 11(a) seem to be a simple sinusoid having a single frequency. The projection analysis (Appendix B) also demonstrates that the local-orbital projection coefficients oscillate with a frequency of ω_{CB} and ω_{DA}, in accordance with the orbital symmetry of b_{2u} and b_{3u}, but irrespective of the QCR components; $|C^{QC}_{b^3_{2u}}|^2$ and $|C^{QR}_{b^3_{2u}}|^2$ oscillate with ω_{CB} whereas $|C^{QC}_{b^2_{3u}}|^2$ and $|C^{QR}_{b^2_{3u}}|^2$ oscillate with ω_{DA}. Figures 11(c) and 11(d) show that $|C^{QC}_{b^3_{2u}}|^2$ and $|C^{QR}_{b^3_{2u}}|^2$ fluctuate with a short time period of $T_{b_{2u}} \sim 5$ ps whereas $|C^{QC}_{b^2_{3u}}|^2$ and $|C^{QR}_{b^2_{3u}}|^2$ fluctuate with a long time period of $T_{b_{3u}} \sim 20$ ps. These estimated time periods are well coincident with those calculated from the energy differences of $T_{DA}=5.69$ ps ($\omega_{DA}=0.798$ meV) and $T_{CB}=21.3$ ps ($\omega_{CB}=0.213$ meV) as found in Fig. 4.

We now consider how the coming-and-going motion is generated in ρ when the electron is injected into the avoided-crossing states. When the avoided crossing is produced by the rational bonding-antibonding interaction (commensurate mixing), the fluctuation in ρ against time is expected to occur only between the QC and QR components because the commensurate mixing places their orbital-node lines coaxially but coincidently in phase. In contrast, when the electron tunnels through the doubly overlapped avoided crossings, such as the point $a2$, some phase shift(s) ($\pi/6$ in $a2$) are generated in their nodal lines. Accordingly, the two interstate interferences shake the electron density not only in the QC↔QR intercomponent direction but also along the QC or QR intracomponent directions. Eventually, a curious rotational motion in ρ^T is induced, as shown in Fig. 12(b) (Ref. 17) (Appendix C) and local dipoles arise in the QCR system, even though the gate potential is applied to the system uniformly. We here calculate the local electric field by solving the TD Poisson equation directly based on the obtained $\rho^T(t)$ and illustrate snapshots at $t \sim$ A, B, and C in Fig. 12(c).[17] We can determine the radially distributed electric field toward the inner center when $t \sim$ A, whereas the direction completely reverses when $t \sim$ B. When $t \sim$ C, the direction and distribution of the local electric field is hard to determine due to the delocalization of the wave function over the QC and QR [Fig. 12(a)]. Thus, the interstate interference in the incommensurately hybridized states generates the coming-and-going motion in ρ (CDW), which causes the complicated fluctuation in the electric field not only in the intercomponent

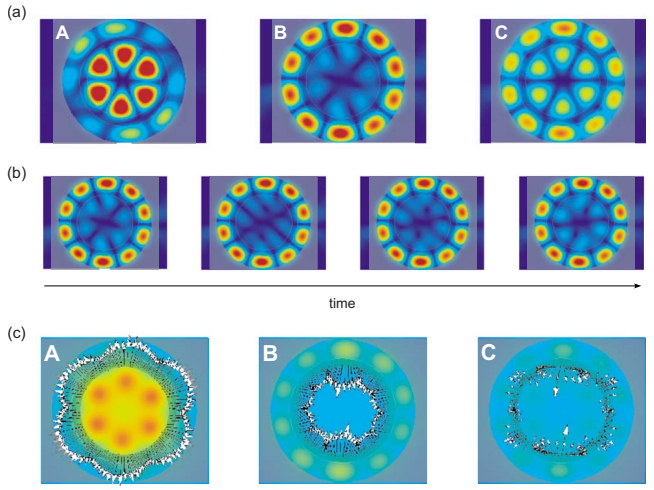

FIG. 12. (Color online) (a) Snapshots of the total charge density ρ^{T} when an electron is asymmetrically injected into the resonant states point $a2$. At time t=A, an electron localizes at the QC area, whereas it localizes at the QR when t=B. An electron delocalizes over the QCR system when t=C. These times t=A, B, and C correspond to those indicated in Fig. 11. (b) Detailed snapshots of ρ^{T} around $t\sim$B, where the charge distribution in the QR does not change, whereas a rotational movement is found in the QC. (c) Snapshots of the electric vectors when t=A, B, and C.

direction but also in the intracomponent directions.

IV. CONCLUSIONS

In this paper we have theoretically studied the resonant tunneling of an electron injected into the QCR multicomponent system. We solved the time-independent Schrödinger equation numerically to determine the eigenstates of an electron confined in the QCR by varying the gate potential. We also solved the time-dependent Schrödinger equation computationally and discussed the dynamical properties of the electron resonant tunneling in this system. The following are new findings based on the calculated results and the discussion by projection analysis.

An observation itself inevitably breaks the initial symmetry of the quantum system and resolves degenerated states into quasidegenerated ones. The present QCR system (D_{2h}) creates two quasidegenerate states in the orbital symmetries of b_{3u} and b_{2u} and in those of a_g and b_{1g}, respectively.

An orbital mixing is induced between the local orbitals of the quantum components when the considered quantum system consists of multicomponents. An application of the electrostatic (gate) potential causes the V independence and linear dependence in the eigenstates. Accordingly, the eigenstates should intersect mutually and creates "crossing and avoided-crossing" points. Electronically, the crossing corresponds to the accidental degeneracy between the local eigenstates whereas the avoided crossing does to the local orbital hybridization.

Owing to the concentric nature of the QCR system, an irrational bonding-antibonding interaction (incommensurate mixing) is found, in addition to the rational bonding-antibonding interaction (the commensurate mixing). Furthermore, the concentricity of the QCR causes the discrepancy in the nodal planes of the local orbitals distinctly and efficiently.

When the electron is injected asymmetrically, the quasidegeneracy in the resulting eigenstates generates interstate interference, which causes a coming-and-going motion in ρ (CDW). Particularly when the electron is injected into the avoided crossing produced by the incommensurate mixing, the interstate interference induces a rotational motion in ρ in spite of the fact that a gate potential is applied uniformly to the system.

The inverse symmetry of the present QCR system (D_{2h}), however, cancels the fluctuation in the local electric field. To extract the net value of the local electric field (local dipole) generated by the electron resonant tunneling we need to modify the geometry of the system.

ACKNOWLEDGMENTS

The authors would like to express their thanks to Shintaro Nomura of University Tsukuba for his fruiful comments, and to Atushi Tsubaki for his kind help in preparing the figures. Parts of the calculations were carried out at Institute for Molecular Science (BUNSHIKEN) Okazaki, Japan. This work is partly supported by the "High-Tech Research Center" Project for Private Universities and a matching fund subsidy from Ministry of Education, Culture, Sports, Science and Technology, Japan (MEXT), 2008.

APPENDIX A: CLASSIFICATION OF CROSSING AND AVOIDED CROSSING

All the resulting eigenstates of the present QCR system are classified into the irreducible representations a_g, b_{1g}, b_{3u}, and b_{2u}, consistent with the system's point-group symmetry of D_{2h}. The former two and the latter two are quasidegenerate because they are degenerate originally in the irreducible representations of Δ_g and Π_u under $D_{\infty h}$ symmetry. Accordingly, three patterns of crossings and two patterns of avoided crossings are predicted in the present QCR system. We summarize these five patterns with their characteristics in Table I.

TABLE I. Classification of the *crossings* and *avoided crossings* in terms of the hybridized LOs.

Pattern	Crossing	Avoided crossing
Single	Nondegenerate LOs	Nondegenerate LOs
Double	Quasidegenerate and nondegenerate LOs	Two sets of quasidegenerate LOs
Quardruple	Two sets of quasidegenerate LOs	

APPENDIX B: PROJECTION ANALYSIS BY QC AND QR LOCAL-ORBITAL EXPANSION

Figure 11(b) reveals that the wave function of the numerically obtained tunneling electron $\Phi^{\mathrm{QCR}}(\mathbf{r},t)$ can be expanded into four QCR resonant states $\phi_m^{\mathrm{QCR}}(\mathbf{r})$ ($m=A$, B, C, and D, as given in Fig. 4) as

$$\Phi^{\mathrm{QCR}}(\mathbf{r},t)=\sum C^m(t)\phi_m^{\mathrm{QCR}}(\mathbf{r})\sim\sum C^m e^{-i\omega_m t}\phi_m^{\mathrm{QCR}}(\mathbf{r}). \tag{B1}$$

Here, we approximate the fluctuation terms in the TD expansion coefficients $C^m(t)$ by the simple harmonic oscillation of the corresponding resonant frequency ω_m, whereas the other TD reductions are included in the coefficients C_m. For simplicity, we express these four resonant states by $|A\rangle=B_{2u}^4$, $|B\rangle=B_{3u}^4$, $|C\rangle=B_{3u}^5$, and $|D\rangle=B_{2u}^5$. The TD wave function $\Phi^{\mathrm{QCR}}(\mathbf{r},t)$ is then approximated in terms of the four resonant states as

$$\Phi^{\mathrm{QCR}}(\mathbf{r},t)=C^{\mathrm{A}}\exp^{-i\omega_{\mathrm{A}}t}|A\rangle+C^{\mathrm{B}}\exp^{-i\omega_{\mathrm{B}}t}|B\rangle+C^{\mathrm{C}}\exp^{-i\omega_{\mathrm{C}}t}|C\rangle+C^{\mathrm{D}}\exp^{-i\omega_{\mathrm{D}}t}|D\rangle. \tag{B2}$$

We further rewrite Eq. (B2) by the QR local orbitals ($|a\rangle=b_{3u}^3$ and $|b\rangle=b_{2u}^3$) and the QC orbitals ($|\alpha\rangle=b_{3u}^2$ and $|\beta\rangle=b_{2u}^2$). Under the typical orbital hybridization these resonant states are represented in terms of the bonding and antibonding states between the local orbitals as

$$\begin{aligned}|A\rangle&=\eta_b^{\mathrm{B}}|b\rangle+\eta_\beta^{\mathrm{B}}|\beta\rangle,\\ |D\rangle&=\eta_b^{\mathrm{A}}|b\rangle-\eta_\beta^{\mathrm{A}}|\beta\rangle,\\ |B\rangle&=\zeta_a^{\mathrm{B}}|a\rangle+\zeta_\alpha^{\mathrm{B}}|\alpha\rangle,\\ |C\rangle&=\zeta_a^{\mathrm{A}}|a\rangle-\zeta_\alpha^{\mathrm{A}}|\alpha\rangle,\end{aligned} \tag{B3}$$

where the notation of the resonant states and the QC and QR local orbitals is the same as that followed in Fig. 4, and the symbols η_i^{I} and ζ_i^{I} indicate the bonding ($I=B$) or antibonding ($I=A$) coefficients for the ith local orbital. The TD wave function $\Phi^{\mathrm{QCR}}(\mathbf{r},t)$ is rewritten by these local orbitals of the QCR component as

$$\Phi^{\mathrm{QCR}}(\mathbf{r},t)=\xi_a|a\rangle+\xi_b|b\rangle+\xi_\alpha|\alpha\rangle+\xi_\beta|\beta\rangle, \tag{B4}$$

where the TD expansion coefficient ξ_i is given as follows:

$$\begin{aligned}\xi_a&=C^{\mathrm{B}}\zeta_b^{\mathrm{B}}\exp(-i\omega_{\mathrm{B}}t)+C^{\mathrm{C}}\zeta_a^{\mathrm{A}}\exp(-i\omega_{\mathrm{C}}t)\\&\equiv K^{\mathrm{B}}\exp(-i\omega_{\mathrm{B}}t)+K^{\mathrm{C}}\exp(-i\omega_{\mathrm{C}}t),\\ \xi_b&=C^{\mathrm{A}}\eta_b^{\mathrm{B}}\exp(-i\omega_{\mathrm{A}}t)+C^{\mathrm{D}}\eta_b^{\mathrm{A}}\exp(-i\omega_{\mathrm{D}}t)\\&\equiv K^{\mathrm{A}}\exp(-i\omega_{\mathrm{A}}t)+K^{\mathrm{D}}\exp(-i\omega_{\mathrm{D}}t),\\ \xi_\alpha&=C^{\mathrm{B}}\zeta_\alpha^{\mathrm{B}}\exp(-i\omega_{\mathrm{B}}t)-C^{\mathrm{C}}\zeta_\alpha^{\mathrm{A}}\exp(-i\omega_{\mathrm{C}}t)\\&\equiv\kappa^{\mathrm{B}}\exp(-i\omega_{\mathrm{B}}t)-\kappa^{\mathrm{C}}\exp(-i\omega_{\mathrm{C}}t),\\ \xi_\beta&=C^{\mathrm{A}}\eta_\beta^{\mathrm{B}}\exp(-i\omega_{\mathrm{A}}t)-C^{\mathrm{D}}\eta_\beta^{\mathrm{A}}\exp(-i\omega_{\mathrm{D}}t)\\&\equiv\kappa^{\mathrm{A}}\exp(-i\omega_{\mathrm{A}}t)-\kappa^{\mathrm{D}}\exp(-i\omega_{\mathrm{D}}t).\end{aligned} \tag{B5}$$

The overlap integral $\Phi^{\mathrm{QCR}}(\mathbf{r};t)$ should be carried out in accordance with the defined area (V=QCR, QC, and QR) as follows:

$$\begin{aligned}\langle\Phi^{\mathrm{QCR}}(\mathbf{r};t)|\Phi^{\mathrm{QCR}}(\mathbf{r};t)\rangle_{\mathrm{V}}&=\xi_a^*\xi_a\langle a|a\rangle_{\mathrm{V}}+\xi_b^*\xi_a\langle b|a\rangle_{\mathrm{V}}\\&+\xi_\alpha^*\xi_a\langle\alpha|a\rangle_{\mathrm{V}}+\xi_\beta^*\xi_a\langle\beta|a\rangle_{\mathrm{V}}\\&+\xi_a^*\xi_b\langle a|b\rangle_{\mathrm{V}}+\xi_b^*\xi_b\langle b|b\rangle_{\mathrm{V}}\\&+\xi_\alpha^*\xi_b\langle\alpha|b\rangle_{\mathrm{V}}+\xi_\beta^*\xi_b\langle\beta|b\rangle_{\mathrm{V}}\\&+\xi_a^*\xi_\alpha\langle a|\alpha\rangle_{\mathrm{V}}+\xi_b^*\xi_\alpha\langle b|\alpha\rangle_{\mathrm{V}}\\&+\xi_\alpha^*\xi_\alpha\langle\alpha|\alpha\rangle_{\mathrm{V}}+\xi_\beta^*\xi_\alpha\langle\beta|\alpha\rangle_{\mathrm{V}}\\&+\xi_a^*\xi_\beta\langle a|\beta\rangle_{\mathrm{V}}+\xi_b^*\xi_\beta\langle b|\beta\rangle_{\mathrm{V}}\\&+\xi_\alpha^*\xi_\beta\langle\alpha|\beta\rangle_{\mathrm{V}}+\xi_\beta^*\xi_\beta\langle\beta|\beta\rangle_{\mathrm{V}}.\end{aligned} \tag{B6}$$

However, the overlap integrals between the local orbitals are reduced to $\langle i|j\rangle=\delta_{ij}$ due to the localized nature and their orthogonality.

Consequently, the partial charge densities ρ^{QR} and ρ^{QC} are given as

$$\begin{aligned}\rho^{\mathrm{QR}}&=\langle\Phi^{\mathrm{QCR}}(\mathbf{r};t)|\Phi^{\mathrm{QCR}}(\mathbf{r})\rangle_{\mathrm{QR}}=|\xi_a|^2+|\xi_b|^2\\&=\sum|K_i|^2+2|K_B^*K_C|^2\cos\omega_{\mathrm{CB}}t+2|K_A^*K_D|^2\cos\omega_{\mathrm{DA}}t,\\ \rho^{\mathrm{QC}}&=\langle\Phi^{\mathrm{QCR}}(\mathbf{r};t)|\Phi^{\mathrm{QCR}}(\mathbf{r})\rangle_{\mathrm{QC}}=|\xi_\alpha|^2+|\xi_\beta|^2\\&=\sum|\kappa_i|^2-2|\kappa_B^*\kappa_C|^2\cos\omega_{\mathrm{CB}}t-2|\kappa_A^*\kappa_D|^2\cos\omega_{\mathrm{DA}}t\\&=\sum|\kappa_i|^2+2|\kappa_B^*\kappa_C|^2\cos(\omega_{\mathrm{CB}}t+\pi)\\&\quad+2|\kappa_A^*\kappa_D|^2\cos(\omega_{\mathrm{DA}}t+\pi).\end{aligned} \tag{B7}$$

Therefore, the total charge density ρ^{T} is given as

$$\rho^{\mathrm{T}}=\langle\Phi^{\mathrm{QCR}}(\mathbf{r};t)|\Phi^{\mathrm{QCR}}(\mathbf{r})\rangle_{\mathrm{QCR}}=|\xi_a|^2+|\xi_b|^2+|\xi_\alpha|^2+|\xi_\beta|^2. \tag{B8}$$

APPENDIX C: ANGULAR MOMENTUM

In order to discuss the rotational fluctuation (along the intracomponent directions) in the charge density, we calculate the expectation value of the angular momentum $\langle l_z\rangle$. As mentioned in Appendix B, the QCR resonant state $\Phi^{\mathrm{QCR}}(\mathbf{r},t)$ is approximately given in the local-orbital expression as

$$\Phi^{\mathrm{QCR}}(\mathbf{r},t)=\xi_a|a\rangle+\xi_b|b\rangle+\xi_\alpha|\alpha\rangle+\xi_\beta|\beta\rangle, \tag{C1}$$

where the expansion coefficient ξ_i is defined in Eq. (B5). The present QCR is a 2D system, so the angular momentum is defined perpendicular to the QCR plane as $\hat{l}_z=-i\hbar\frac{\partial}{\partial\theta}$. The expectation values of the partial angular momentum $\langle l_z\rangle^{\mathrm{P}}(=\langle\Phi^{\mathrm{QCR}}(\mathbf{r},t)|\hat{l}_z|\Phi^{\mathrm{QCR}}(\mathbf{r},t)\rangle_{\mathrm{V}}$; P,V=QR or QC) are then given by the local-orbital expression [Eq. (C1)] as

$$\langle l_z\rangle^{\mathrm{QR}}=|\xi_a|^2\langle a|\hat{l}_z|a\rangle_{\mathrm{QR}}+|\xi_b|^2\langle b|\hat{l}_z|b\rangle_{\mathrm{QR}}+\xi_a^*\xi_b\langle a|\hat{l}_z|b\rangle_{\mathrm{QR}}+\xi_b^*\xi_a\langle b|\hat{l}_z|a\rangle_{\mathrm{QR}}, \tag{C2}$$

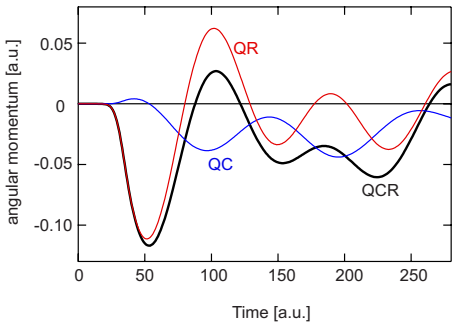

FIG. 13. (Color online) Calculated expectation value of the partial and total angular momenta, perpendicular to the QCR plane. The electron is injected asymmetrically into the avoided-crossing state $a2$ of the QCR (Figs. 11 and 12), though with a slight change in the potential height (V_{QC}=0.02 a.u.) to allow effective tunneling into the QC area. This modification does not cause any essential change in the TD feature of the partial $\langle l_z\rangle^{\mathrm{QC}}$, $\langle l_z\rangle^{\mathrm{QR}}$, and total $\langle l_z\rangle^{\mathrm{T}}$ values. The time for 1 a.u. is equal 56.68 fs in this effective atomic unit system.

$$\langle l_z\rangle^{\mathrm{QC}} = |\xi_\alpha|^2\langle\alpha|\hat{l}_z|\alpha\rangle_{\mathrm{QC}} + |\xi_\beta|^2\langle\beta|\hat{l}_z|\beta\rangle_{\mathrm{QC}} + \xi_\alpha^*\xi_\beta\langle\alpha|\hat{l}_z|\beta\rangle_{\mathrm{QC}} + \xi_\beta^*\xi_\alpha\langle\beta|\hat{l}_z|\alpha\rangle_{\mathrm{QC}}. \tag{C3}$$

The sum of these partial values gives the total value

$$\langle l_z\rangle^{\mathrm{T}} = \langle\Phi^{\mathrm{QCR}}(\mathbf{r},t)|\hat{l}_z|\Phi^{\mathrm{QCR}}(\mathbf{r},t)\rangle_{\mathrm{QCR}} = \langle l_z\rangle^{\mathrm{QC}} + \langle l_z\rangle^{\mathrm{QR}}. \tag{C4}$$

We show the calculated values of these partial and total angular momenta in Fig. 13. If the QCR system has a strict point-group symmetry of $D_{\infty h}$, the QR and QC local orbitals $|a\rangle$, $|b\rangle$ and $|\alpha\rangle$, $|\beta\rangle$ are the eigenstates of $\hat{l}_z$, and the angular part of their wave functions is proportional to $\exp(il\theta)$, as mentioned in Sec. II. Then, the cross terms in Eqs. (C2) and (C3) should disappear and the resulting TD feature of $\langle l_z\rangle^{\mathrm{QR}}$ and $\langle l_z\rangle^{\mathrm{QC}}$ is coincident with that found in the corresponding partial densities. That is, both fluctuate with a characteristic frequency derived from ω_{CB} and ω_{DA} determined by the energy difference in the resonant states having the same orbital symmetry (Fig. 4). This is why $\langle l_z\rangle^{\mathrm{QR}}$ and $\langle l_z\rangle^{\mathrm{QC}}$ fluctuate with the opposite phase from π (Fig. 13). However, the lowered geometrical symmetry in the present QCR system breaks the local orbitals so they become eigenstates of $\hat{l}_z$. Consequently, the crossing terms of $\langle a|\hat{l}_z|b\rangle_{\mathrm{QR}}$, $\langle\alpha|\hat{l}_z|\beta\rangle_{\mathrm{QC}}$, etc., remain finite values, which induces other frequency components in the expectation values of the partial angular momenta. These values are determined by the difference in the resonant frequencies having different orbital symmetries, such as ω_{BA}, ω_{CA}, ω_{DB}, and ω_{DC}.

*Present address: Center for Interdisciplinary Research, Tohoku University.
†takeda@waseda.jp

[1] For example, S. Viefers, P. Koskinen, P. Singha Deo, and M. Manninen, Physica E **21**, 1 (2004).
[2] Y. Aharonov and D. Bohm, Phys. Rev. **115**, 485 (1959).
[3] A. Tonomura, N. Osakabe, T. Matsuda, T. Kawasaki, J. Endo, S. Yano, and H. Yamada, Phys. Rev. Lett. **56**, 792 (1986).
[4] J. M. Garcia, G. Medeiros-Ribeiro, K. Schmidt, T. Ngo, J. L. Feng, A. Lorke, J. Kotthaus, and P. M. Petroff, Appl. Phys. Lett. **71**, 2014 (1997).
[5] V. Chandrasekhar, R. A. Webb, M. J. Brady, M. B. Ketchen, W. J. Gallagher, and A. Kleinsasser, Phys. Rev. Lett. **67**, 3578 (1991).
[6] D. Mailly, C. Chapelier, and A. Benoit, Phys. Rev. Lett. **70**, 2020 (1993).
[7] T. Okunishi, Y. Ohtsuka, M. Muraguchi, and K. Takeda, Phys. Rev. B **75**, 245314 (2007).
[8] A. Lorke, R. J. Luyken, A. O. Govorov, J. P. Kotthaus, J. M. Garcia, and P. M. Petroff, Phys. Rev. Lett. **84**, 2223 (2000).
[9] D. Granados, J. M. Garcia, T. Ben, and S. I. Molina, Appl. Phys. Lett. **86**, 071918 (2005).
[10] T. Mano, T. Kuroda, S. Sauinetti, T. Ochiai, T. Tateno, J. Kim, T. Noda, M. Kawabe, K. Sakoda, G. Kido, and N. Koguchi, Nano Lett. **5**, 425 (2005).
[11] M. Muraguchi and K. Takeda, Jpn. J. Appl. Phys., Part 1 **46**, 1224 (2007).
[12] Normally, the application of a gate potential to an insulator (potential barrier) creates a complicated potential profile such as a depletion layer and an electric double layer. However, for simplicity we here neglect the reduction in the applied gate potential in the barrier which separates the QC and QR components from the QCR system and assume that the net value of the applied gate potential causes a uniform difference between the relative local eigenstates.
[13] Originally, the resonant states having orbital symmetry b_{3u} and b_{2u} are degenerate in the Π_u state under the point-group symmetry $D_{\infty h}$. Strictly, at the resonant state $T1$, the energy eigenvalues of B_{3u}^4 and B_{2u}^4 do not coincide whereas they both cross the resonant state A_g^3 (Appendix A).
[14] We inject the electron as a Gaussian-type wave packet having an even (cosinusoidal) orbital symmetry in the y direction (perpendicular to the electron propagation). We note that both resonant states A_g^6 and B_{3u}^4 have an even parity in the y direction whereas the eigenstate B_{2u}^4 has an odd parity. Thus, the symmetrically injected electron tunnels through the QCR system via the resonant states A_g^6 and B_{3u}^4 while the resonant state B_{2u}^4 is excluded from resonant tunneling under the present symmetrical injection.
[15] Under the point-group symmetry D_{2h}, the latter two states B_{3u}^4 and B_{2u}^4 are originally degenerate (e_u representation) under $D_{\infty h}$ symmetry. The lowered geometrical symmetry in the QCR system resolves the degeneracy and causes a quasidegeneracy. Accordingly, strictly accidental degeneracy occurs between the resonant states A_g^3 and B_{3u}^4 or A_g^3 and B_{2u}^4, where any hybridization occurs.
[16] We set the central velocity of the injected electron wave packet at 0.44 nm/fs to give an initial kinetic energy of 48.3 meV. Figure 11(b) shows that the injected electron tunnels via all the

resonant states in the order B^5_{2u}, B^4_{2u}, B^4_{3u}, and finally B^5_{3u}. When an electron is asymmetrically injected into the crossing point $T1$, $|C_i^{\mathrm{QCR}}|^2$ coincides with $|C_i^{\mathrm{QR}}|^2$ or $|C_i^{\mathrm{QC}}|^2$ (Fig. 10). However, the present injection into $a2$ does not give rise to agreement among these projection coefficients nor between the partial charge densities (ρ^{QR} and ρ^{QC}) and the projection coefficients ($|C_i^{\mathrm{QCR}}|^2$). The only agreement is found between ρ^{QC} and $|C_i^{\mathrm{QC}}|^2$ and between ρ^{QR} and $|C_i^{\mathrm{QR}}|^2$ [Figs. 11(a), 11(c), and 11(d)]. This is because $|C_i^{\mathrm{QCR}}|^2$ are not necessarily in agreement with $|C_i^{\mathrm{QR}}|^2$ or $|C_i^{\mathrm{QC}}|^2$ when the electron is injected into the avoided-crossing point (Appendix B).

[17] See supplementary material at http://link.aps.org/supplemental/10.1103/PhysRevB.81.115309 for corresponding movies.